Journal Pre-proof

Mathematical modelling of injection time in autoinjectors: State of the art and future perspectives

Andrea Friso, Mark Palmer, Federico Galvanin

PII: S0378-5173(25)01287-6
DOI: https://doi.org/10.1016/j.ijpharm.2025.126450
Reference: IJP 126450

To appear in: *International Journal of Pharmaceutics*

Received date : 25 July 2025
Revised date : 5 November 2025
Accepted date : 29 November 2025

Please cite this article as: A. Friso, M. Palmer and F. Galvanin, Mathematical modelling of injection time in autoinjectors: State of the art and future perspectives. *International Journal of Pharmaceutics* (2025), doi: https://doi.org/10.1016/j.ijpharm.2025.126450.

Mathematical Modelling of Injection Time in Autoinjectors: State of the Art and Future Perspectives

Andrea Friso[a], Mark Palmer[b], Federico Galvanin[a]

[a] *Department of Chemical Engineering, University College London, Torrington Place, London, WC1E7JE, United Kingdom*
[b] *GlaxoSmithKline, Park road, Ware, SG120DP, United Kingdom,*

Abstract

Autoinjector devices are a specialised type of medical equipment used for the self-administration of medications. Over the past decade, the significance in these devices has increased, both in terms of their usage and academic interest. An important parameter to be characterised in these devices is the injection time, defined as the duration required to deliver the correct amount of medication. Due to the growing interest in autoinjectors, there has been a pressing need to develop mathematical models for their design and optimization. This review paper presents an analysis of the different mathematical models used to understand and describe autoinjectors devices. Models are analysed, with key characteristics highlighted to showcase the advantages and disadvantages of each in different applications. In comparing these models, the trade-off between accuracy and precision of the predictions are discussed, as well as the importance of validating the models under different conditions. The implications for future research in this field are discussed, emphasizing the need for improved parameter estimation and standardized validation protocols. By addressing current limitations and leveraging advancements in technology, such as multi-physics modelling and machine learning, the field can advance toward more effective and reliable autoinjector designs, ultimately improving patient outcomes and expanding the utility of these devices.

Keywords: autoinjectors, hydrodynamic force, friction force, injection time

1. Introduction

Autoinjectors are medical devices designed for the self-administration of injectable drugs (Sicherer et al., 2007; Simons and Simons, 2010; Roy et al., 2021). In recent years, their use has seen a marked increase, driven by a rise in diagnoses of diabetes (Figure 1a) and other chronic diseases (Rowley et al., 2017; Ong and Stafford, 2023). This surge is also fuelled by the development of protein-based medicines, such as biologics, which cannot be ingested due to enzymatic degradation and poor bioavailability in the gastrointestinal tract (Renukuntla et al., 2013). This trend is further reflected in the growing academic interest in injection tolerability, suitability for self-administration, and pharmacokinetic equivalence (Figure 1b).

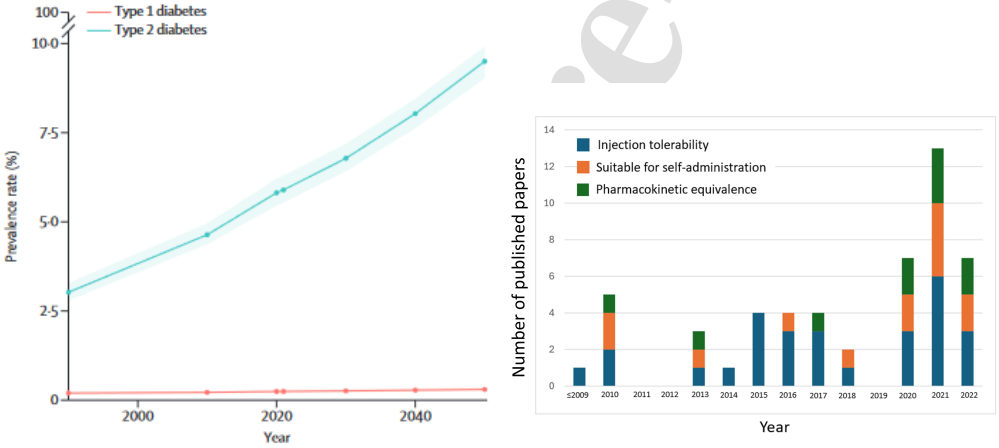

(a) (b)

Figure 1: (a) Worldwide age-standardized prevalence projections for type 1 and type 2 diabetes from 1990 to 2050 (Ong and Stafford, 2023). (b) Evolution of the previous research on subcutaneous drug deliver, organised in three themes: injection tolerability, suitability for self-administration and pharmacokinetic equivalence (Schneider et al., 2023).

The increasing popularity of autoinjectors is attributable to their convenience, which allows patients to administer medications without the need for medical expertise (Stiefel et al., 2020; Ross et al., 2025). Currently, more than 20 pharmaceutical companies have developed over 70 different types of autoinjectors, each varying in dimensions and shapes (Figure 2).

Given their significant role in drug delivery, the importance of optimizing autoinjectors cannot be overstated. These devices offer a reliable and

Figure 2: Range of auto injector and pen injector solutions that can accommodate changing injection needs such as higher viscosity, larger volumes (Shilpa et al., 2022).

user-friendly means of administering essential medications, thus improving treatment adherence and overall health outcome. The demand for effective autoinjectors has increased, driven by the increase in chronic conditions that require regular injections, such as diabetes, rheumatoid arthritis, multiple sclerosis (Sicherer et al., 2007), and anaphylaxis (Dribin et al., 2023). Furthermore, the increasing incidence of severe allergic reactions, which requires immediate administration of epinephrine, underscores the critical role of these devices. Thus, optimizing auto-injector performance is crucial. The key parameter to characterise in these systems is the injection time, i.e., the duration required to deliver the correct dosage of medication which directly affects both the efficacy and comfort of the drug delivery process. Precise control of injection time is essential to ensure that the medication is administered at the optimal rate, maximizing therapeutic benefits while minimizing discomfort and potential complications.

Mathematical models have become indispensable in the design and development of autoinjectors (Rathore et al., 2011; Zhong et al., 2021, 2022b; Thueer et al., 2018). These models enhance the understanding and prediction of the forces and dynamics involved in the injection process, supporting the optimisation of device components and operational parameters. By accurately modelling the injection process, researchers can design more efficient, reliable, and user-friendly autoinjectors. This review paper aims to provide a comprehensive analysis and comparison of various mathematical models

used to describe friction forces in autoinjectors. The work highlights the strengths and limitations of each model and discusses their applicability in different injection scenarios. By examining these models, the review underscores the importance of reliable modelling in advancing autoinjector technology. The paper presents literature models, illustrating their characteristics, advantages, and limitations. It also discusses the practical implications for researchers, emphasising the need for improved parameter estimation and standardised validation protocols (Zhong et al., 2021; Kennelly et al., 2024). In addition, the review explores future research directions, including the development of dynamic friction models and the integration of advanced computational techniques, such as machine learning or hybrid modelling, into standard modelling methodologies. This review aims to demonstrate the progress made in autoinjector modelling, while identifying areas that require further innovation and improvement. By addressing current limitations and leveraging technological advancements, the field can advance towards more effective and reliable devices, ultimately improving patient outcome and expanding the utility of autoinjectors. The paper is structured as follow: Section 2 explains the structure of autoinjectors and the forces acting during the injection process; Section 3 presents and describes the traditional models used to characterize these forces; Section 4 explores the most recent innovative models, including those not yet applied to characterize the main forces acting on the system; Section 5 provides a comparative analysis of the candidate models; Section 6 compares the injection times calculated using the models discussed in Section 5; Section 7 discusses potential directions for future work; and finally, Section 8 presents the conclusions of this paper.

2. Background

This review aims to provide a comprehensive overview of the current state-of-the-art in the field of autoinjectors, highlighting not only the fundamental operating principles but also recent advances and emerging trends in their mathematical modelling. The rapid rise in the adoption of autoinjectors in clinical and home settings is closely linked to the growing prevalence of chronic diseases, patient preference for self-administration, and the need for rapid emergency treatment (Dostal et al., 2023). Several types of autoinjectors are currently available on the market but the most common type utilizes a pre-loaded spring as power source (Ravi et al., 2015; Dostal et al., 2023). Recent reviews report that more than 20 pharmaceutical companies

have developed approximately 80 autoinjector models to date, with over 50 medicines delivered via such devices (Dostal et al., 2023). The market trend is towards increasing device usability, single-handed operation, and suitability for a broader range of drugs, including high-viscosity formulations and large-volume biologics (Dostal et al., 2023; Masciopinto, 2024). A schematic representation of this device's structure is shown in Figure 3, illustrating the following key parts. The numbers in brackets correspond to the numbered components shown in Figure 3.

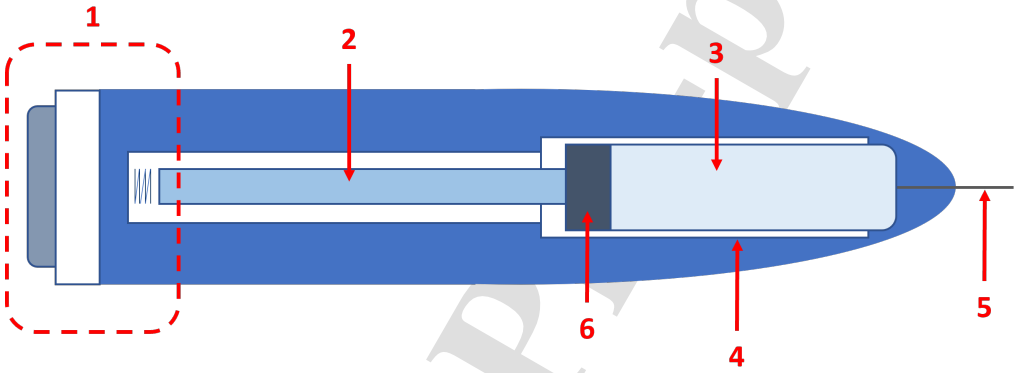

Figure 3: Structure of the spring-driven autoinjector.

- Activation mechanism [1]: provides the power required for the injection. This mechanisms includes the activation button, which releases the spring that delivers the injection energy.
- Plunger [2]: a movable component that transfers the elastic energy of the spring into kinetic energy.
- Primary pack [3]: contains the medication that has to be administered. Its size may vary depending on the type of drug. It includes also a cylindrical part that provides structural support [4].
- Needle [5]: used to pierce the patient's tissue and deliver the medication to the designated area.
- Stopper [6]: prevents medication from leaking and spilling out of the cartridge.

The design of autoinjectors varies depending on their function and the type of medication they administer. Over time, autoinjector design has evolved to include innovative mechanical solutions and improved ergonomics, reflecting both technological advancements and the feedback from extensive post-market surveillance (Masciopinto, 2024; Zhong et al., 2023). The simplest type of autoinjector follows a straightforward injection procedure comprising three main steps:

1. The patient inserts the needle into the designated area of he body.
2. The activation button is pressed, releasing the spring and initiating the plunger's movement, which inject the medication. The spring is released and the plunger starts to move injecting the medication.
3. The plunger reaches the end of its travel marking the completion of the injection.

In more complex autoinjectors, like the one shown in Figure 4 a dual movement of the syringe barrel is required and the activation procedure involves two distinct steps:

1. The activation button triggers a mechanism that pushes the syringe, causing the needle to pierce the patient skin. This movement is the one marked as 1 in Figure 4.
2. The spring is then activated, initialising the injection procedure, movement 2 in Figure 4.

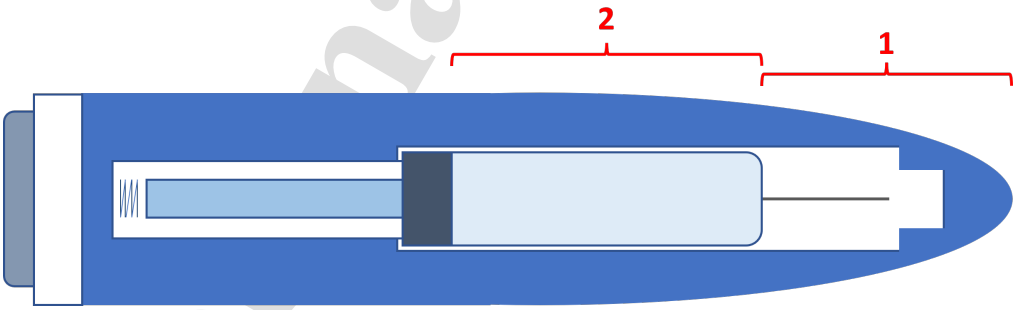

Figure 4: Structure of the two-movements spring-driven autoinjector.

This evolution towards more sophisticated devices is indicative of ongoing trends in the field: the incremental integration of safety, dual-step mechanisms for precision, and feedback-driven innovation responding to clinical

and user needs (Dostal et al., 2023; Zhong et al., 2023). These more complex devices require a dual movement of the syringe plunger. During injection procedure, the device can reach acceleration close to 1000 m/s^2 (Zhong et al., 2023, 2021). Such rapid acceleration can cause significant pressure variations within the fluid inside the syringe cartridge, potentially leading to the formation of protein aggregates which can result in in cellular toxicity and other advert effects (Riesz and Kondo, 1992; Torisu et al., 2017; Li et al., 2020). This additional complexity makes modelling these types of autoinjectors more challenging.

2.1. Overview of forces acting during the injection procedure

The literature increasingly focuses on understanding and modelling the forces acting during autoinjector operation, as their interplay is central to device performance and patient safety (Derakhshandeh et al., 2025; Dostal et al., 2023). Figure 5 provides an overview of these forces during the injection process.

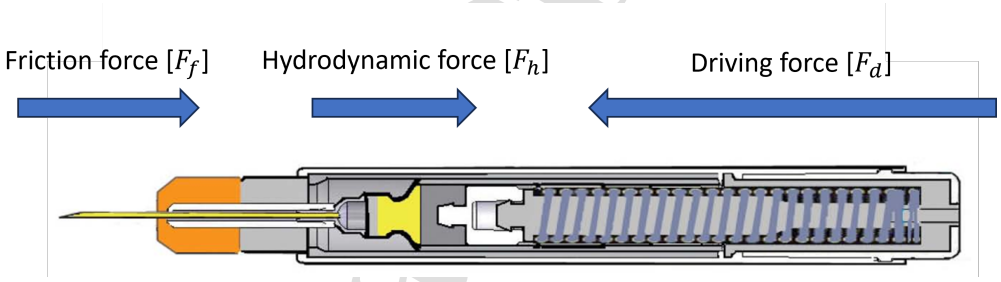

Figure 5: Schematic representation of the forces acting on the autoinjector (Shaik et al., 2016).

As shown in Figure 5 the three primary forces acting on the autoinjector are:

- Driving force [F_d]: mechanical energy required to perform the injection.
- Hydrodynamic force [F_h]: resistance force generated by the resistance of the fluid.
- Friction force [F_f]: resistance force generated by the contact between the inner wall of the syringe and the syringe plunger.

The subsequent sections will explain the physical meaning and insights on the relative role of these forces.

2.1.1. Driving force

The driving force, F_d, in autoinjector refers to the mechanical force that provides the energy required for the injection process. This force is crucial as it must counteract the forces resisting injection, i.e. friction and hydrodynamic forces. The primary function of the driving force is to ensure that the medication is delivered at the appropriate pressure and within the required time frame. Autoinjectors available on the market utilize various mechanisms to generate the driving force:

- Spring mechanism: the most common driving mechanism, where a compressed spring in the device's top part is released using an activation button. The magnitude of the force depends on the spring's characteristic, typically ranging from 8 to 50 N (Fischer et al., 2015; Zhong et al., 2022a).

- Gas propellant: a less common mechanism where a gas, such as compressed air or carbon dioxide, is stored within the device and released upon activation, creating a pressure gradient that moves the plunger (Badkar et al., 2021).

- Mechanical assistance: in this mechanism, the primary energy source is provided by the user and then amplified by an internal mechanical system (Barone et al., 2016).

- Spring-assisted gas: a combination of spring and gas propellant mechanism (McCawley and Lavin, 2023). In this setup, the gas initiates the injection, but the main power source is the spring.

This paper focuses on the spring-driven mechanism, as it is the most common mechanism encountered in commercial autoinjector devices. The design considerations for this mechanism include factors such as the medication's viscosity, the desired injection time, and user comfort.

2.1.2. Hydrodynamic force

Recent literature reviews place significant attention on the fluid dynamics of autoinjector administration, emphasizing that the emergence of high concentration biologics requires detailed rheological characterization and modelling to prevent aggregation and ensure reliable dosing (Allmendinger et al.,

2014; Zhong et al., 2023).The hydrodynamic force, F_h, in autoinjectors is generated by the flow of medication through the syringe and out of the needle during injection. This force is governed by the principles of fluid dynamics. Specifically, when the device is activated and the driving force is applied, resistance arises due to the rheological properties of the fluid, such as viscosity and density, as well as the geometrical properties of the device. An important consideration in understanding hydrodynamic forces is the type of fluid to be injected. A number of drugs administered via autoinjectors are protein-based or amino acid derivatives. Experimental studies have shown that certain monoclonal antibodies, which are protein-based drugs, exhibit a constant viscosity at low shear rates but demonstrate shear-thinning behaviour at higher shear rates (Allmendinger et al., 2014). Consequently, it is crucial to study the influence of the fluid's rheological properties on the hydrodynamic forces (Zarraga et al., 2013; Zhong et al., 2022b; Scherer et al., 2010).

2.1.3. Friction force

Multiple comparative studies in the field underline the impact of material selection, lubrication strategies, and frictional regimes on device performance and reliability, highlighting this as a persistent research focus for next generation autoinjectors (Sree et al., 2023; Rathore et al., 2011; Derakhshandeh et al., 2025). A key force opposing the driving force in autoinjectors is the friction force, F_f. This force is a fundamental concept in the physics of autoinjectors, describing the resistance encountered when two surfaces are in contact and sliding against each other (Al-Bender, 2010). The friction force plays a crucial role in many scientific and engineering applications, impacting the performance, efficiency, and reliability of systems (Zhong et al., 2021). Understanding the mechanism underlying friction is essential for optimizing and design systems involving contact interactions between two surfaces. In the context of autoinjectors, friction arises from the interactions between the walls of the stopper and the inner wall of the syringe barrel. this force is influenced by several factors, including the material of the autoinjector components, the presence of a silicone lubricant layer, and the thickness of this layer (Rathore et al., 2011). Examining the sliding process reveals two distinct frictional regimes:

- Pre-sliding regime: in this regime, adhesive forces between the asperities (microscopic contact points) of the two surfaces dominate. Consequently, the friction force is primarily a function of surface displacement

rather then velocity. The asperities deform in an elastic-plastic manner, causing the surfaces to behave like a non-linear hysteretic spring.

- Gross sliding regime: this regime occurs when displacement increases significantly, causing the junctions between asperities to break more frequently and reform less often. The term "gross" refers to the relatively free sliding of the surfaces, accompanied by a high degree of frictional resistance.

The transition between these regimes depends on the relative velocity of the two surfaces, which characterises the process of asperities formation and breaking (Daniel, 1992).

3. Conventional Mathematical Models for Autoinjectors

In this section the most used models to describe the autoinjector forces introduced in Section 2.1 are described. The assumptions used to calibrate, study and compare the models i the next sections are:

- All models are calibrated using experimental data obtained from "in air" injections, meaning they do not account for subcutaneous tissue resistance nor for physiological back pressure effects presented in clinical scenarios.

- Hydrodynamic resistances and fluid mechanics are calculated under the assumption of Newtonian behaviour and constant viscosity.

- All models treat spring mechanics and component tolerances (such as plunger fit and lubricant layer) as idealized, consistent throughout the injection, with no empirical variation considered.

A summary of these assumptions is reported in Table 1.

3.1. Rathore model

In the study by Rathore et al. (2011), the authors investigate the role of each component of autoinjectors (barrel, stopper, silicone layer and needle), estimate their variability, and evaluate their impact on the forces and injection time. This study used syringes from different vendors, as detailed in Table 2 to assess the variability in the syringe components and its impact on the injection forces.

Table 1: Summary of main assumptions for each autoinjector model. ✓: assumption present, ×: assumption not considered. For 'variable friction', models allow friction to change with velocity or force; 'constant' means it does not.

Assumption	Rathore	Zhong	SZhong	LuGre
Calibrated in air	✓	✓	✓	✓
Tissue back pressure	×	×	×	×
Friction constant	✓	×	×	×
Hydrodynamics in air	✓	✓	✓	✓
Spring ideal mechanics	✓	✓	✓	✓
Device tolerance fixed	✓	✓	✓	✓
Viscosity constant	✓	✓	✓	✓

Table 2: List of syringe types used in the work of Rathore et al. (2011).

Syringe vendor	Syringe type
Vendor 1	Siliconized glass
Vendor 2	Siliconized glass
Vendor 3	Siliconized glass
Vendor 4	Plastic

The forces acting during the injection were measured using an Instron material testing system (Instron, 2025) reported in Figure 6. The Inston offers precise control and measurement of the forces involved in the syringe operation, ensuring reliable and repeatable results. This instrument operates by applying a controlled displacement or force to the syringe plunger while continuously measuring the resulting force or displacement. By controlling the speed and position of the plunger, the Instron can accurately simulate real-use conditions, allowing for detailed analysis of the extrusion force profile throughout the injection process. The data collected can be used to evaluate factors such as break-loose force, glide force, and consistency of delivery, providing valuable insights for device optimization and quality control.

Using the setup shown in Figure 6, the driving force required to deliver a fixed amount of medication was characterised. The force balance used in their analysis is described by Equation 1 where F_d is the driving force, F_h is the hydrodynamic force, and F_f is the friction force.

$$F_d = F_h + F_f \tag{1}$$

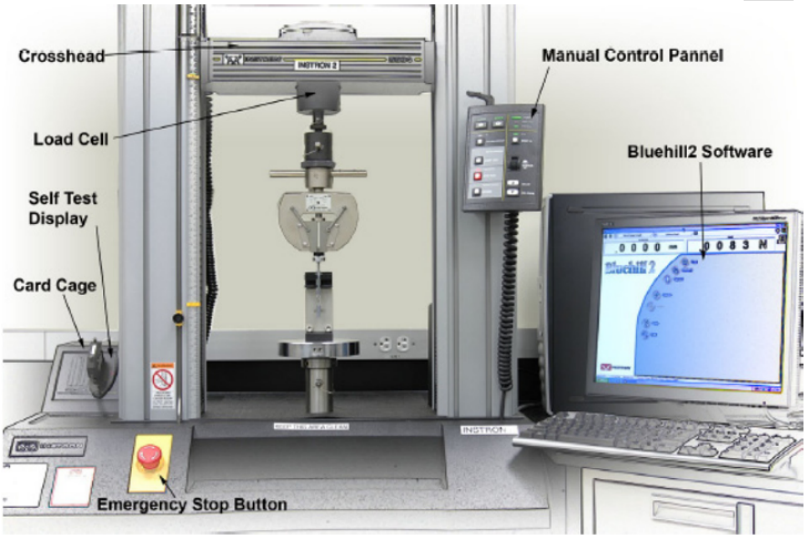

Figure 6: Instron system used for measuring extrusion forces (Rathore et al., 2011).

The friction force is defined as follow:

$$F_f = \left(\frac{2\pi \mu_{oil} r_b L_{stopper}}{d_{oil}} \right) \bar{v} = K_f \bar{v} \tag{2}$$

Where μ_{oil} is the viscosity of the lubricating oil, d_{oil} is the effective thickness of the lubricant layer between the stopper and the syringe, L_{stopper} is the length of the stopper in contact with the syringe walls, r_b is the radius of the barrel, and $\bar{v}$ is the average injection speed. It should be noted that d_{oil} represents the actual thickness of the oil layer during injection, which may differ from the applied lubrication thickness due to displacement of oil by the stopper as it moves along the syringe. Insufficient lubrication can result in smaller d_{oil} values, increasing frictional resistance. The equation illustrates the relationship between friction force and injection speed, showing that F_f is directly proportional to the average injection speed, $\bar{v}$, as expressed by $F_f = K_f \bar{v}$. The proportionality constant K_f encapsulates the effects of the lubricant viscosity (μ_{oil}), the effective lubricant layer thickness (d_{oil}), the barrel radius (r_b), and the stopper length (L_{stopper}). For example, a higher viscosity or a longer stopper increases frictional resistance, thus increasing K_f. In contrast, a thicker effective lubricant layer reduces friction force. This linear dependence assumes a homogeneous and constant lubri-

cant layer, implying predictable lubricant behaviour under varying injection speeds. However, parameters such as d_{oil} and L_{stopper} are challenging to measure directly and may vary during injection due to deformation, lubrication redistribution, or oil displacement, potentially invalidating these simplifying assumptions.

The hydrodynamic force, F_h, appearing in Equation 1 is expressed as

$$F_h = \left(\frac{8\pi\mu_F L_n r_b^4}{r_n^4} \right) \bar{v} = K_h \bar{v} \tag{3}$$

In this equation, μ_F represents the viscosity of the fluid to be injected, L_n is the needle length, r_b and r_n are the radii of the barrel and the needle, respectively, and $\bar{v}$ is the average injection speed. The hydrodynamic force's linear dependence on injection speed is captured by the constant K_h. By combining Equations 2 and 3, the total driving force necessary for the injection process is derived:

$$F_{driven} = \left(\frac{2\pi\mu_{oil} r_b l_{stopper}}{d_{oil}} \right) \bar{v} + \left(\frac{8\pi\mu L_n r_b^4}{r_n^4} \right) \bar{v} \tag{4}$$

To obtain the injection time, the momentum balance must be defined, as shown in Equation 6:

$$m_{stopper} \frac{d^2x}{dt^2} = k(l_0 - x) - K_f \frac{dx}{dt} - K_h \left(\frac{dx}{dt} \right)^n \tag{5}$$

Here, K_f and K_h are the frictional and hydrodynamic constants derived in Equations 2-3, $m_{stopper}$ is the stopper mass, n is the power law viscosity index of the liquid, x is the compressed length of the spring, l_0 is the free length of the spring, and k is the spring constant. For a Newtonian fluid with $n = 1$, an analytical approximation can be derived starting from Equation **??**:

$$x(t) = l_0 + (x_0 - l_0)\exp\left[\left(\frac{-k}{K_f + K_h} \right) t \right] \tag{6}$$

For a non-Newtonian fluid, where $n \neq 1$, the authors assumed that the friction force lies in the range from 1 to 3 N across various injection velocities. With this assumption, the friction force can be considered constant and equal to C_f, leading to the following analytical solution:

$$x(t) = c_0 + \left[-\left(\frac{n-1}{n}\right)\frac{k}{K_h}t + (x_0 - c_0)^{(n-1)/n} \right]^{n/(n-1)} \quad (7)$$

where c_0 is defined by:

$$c_0 = l_0 - C_f/k \quad (8)$$

This model provides a comprehensive framework for understanding the forces involved in the injection process. The assumptions made, such as the homogeneity of the silicone layer and the approximation of the friction force, simplify the complex interactions within the syringe. The linear dependence of friction and hydrodynamic forces on injection speed offers valuable insights into optimising autoinjector devices.

To contextualise Rathore's model, it is beneficial to compare it with other models used in this field. For example, other models include more detailed considerations of non-Newtonian fluids behaviour or the effects of varying syringe materials. Highlighting these comparisons can illustrate the strengths and potential limitations of Rathore's model, providing a comprehensive perspective on its application in autoinjector design.

3.2. Zhong model

In the work of Zhong et al. (2021), the authors developed a model to describe the injection time for spring-driven autoinjectors. Unlike the model discussed in Section 3.1, this system is more complex due to the dual movement of the barrel and the plunger (described in Section 2). A schematic representation of this device and its components is shown in Figure 7.

To develop the model, the authors divided the system into three units: the spring-rod, the plunger, and the syringe (Figure 8), and analysed the forces acting on each component.

The force balance for spring-rod component is given by Equation 9.

$$F_{spring} - F'_f - F_{rp} = (m_{spring} + m_r)a_r \quad (9)$$

Here F_{spring} is the spring force, m_r is the rod mass, a_r is the rod acceleration, m_{spring} is the effective mass of the spring (taken as 1/3 of its nominal mass Fox and Mahanty (1970)), F'_f is the friction force within the spring-rod component, and F_{rp} is the force applied by the plunger when impacted by the rod. The forces acting on the plunger, illustrated in Figure 8(b), are described by Equation 10:

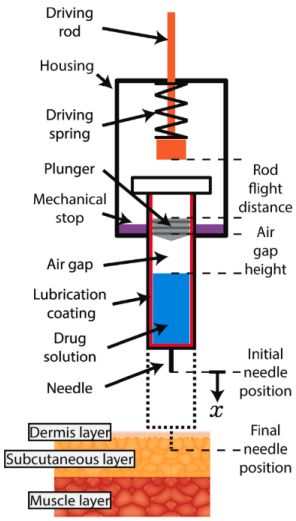

Figure 7: Standard configuration of a spring-driven autoinjector with a dual movement.

$$F_{rp} - F_f'' + \frac{\pi}{4} d_b^2 (p_{atm} - p_{ag}) = m_p a_p \tag{10}$$

where d_b is the barrel diameter, p_{ag} is the instantaneous pressure within the air-gap, F_f' is the friction force on the plunger, p_{atm} is the atmospheric pressure, and m_p and a_p are the mass and acceleration of the plunger, respectively. For the syringe barrel, shown Figure 8(c), the force balance is given by Equation 11:

$$F_f'' + \frac{\pi}{4} d_b^2 (p_{ag} - p_{atm}) - F_{bs} = (m_b + m_l + m_n) a_b \tag{11}$$

Here m_b, m_l, and m_n are the mass of the barrel, the mass of the liquid, and the mass of the needle, respectively, a_b is the barrel acceleration, and F_{bs} is the force due to the contact between the stopper and the barrel. Assuming that the Reynolds number is generally smaller than 2000 (Pritchard, 2010), it is possible to assume laminar flow in the needle. Consequently, an Hagen-Poiseuille velocity profile in the needle can be considered (Thueer et al., 2018).

Given these assumptions, the momentum balance in the autoinjector, if the needle is partially filled, is described by Equation 12:

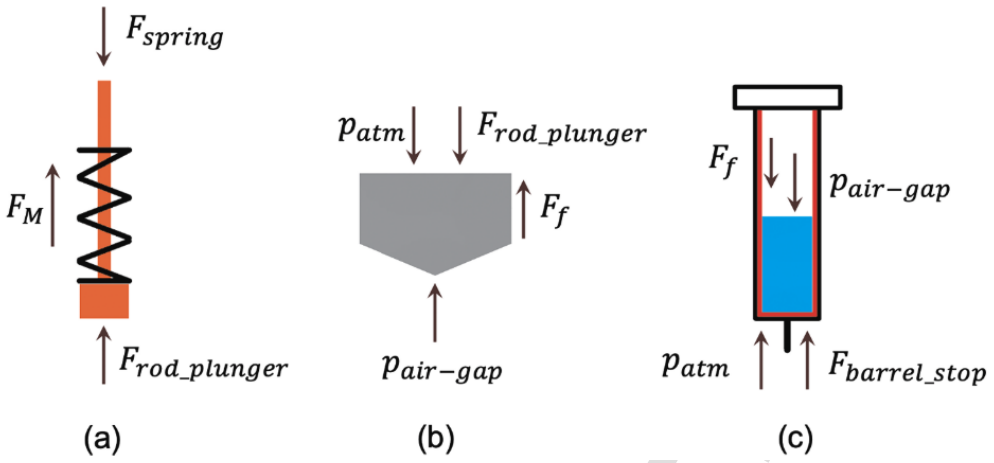

Figure 8: Autoinjector component units: (a) spring-rod, (b) plunger, and (c) syringe.

$$\frac{d}{dt}\left(\frac{\pi}{4}d_n^2\rho_l h_{l2} v_{l2}\right) = \frac{\pi}{4}d_n^2\left(p_{tn} - p_{atm}\right) - \frac{\pi}{4}d_n^2\rho_l a_b h_{l2} \; - 8\pi\mu_l v_{l2} h_{l2} + \frac{\pi}{4}d_n^2\rho_l v_{l2}^2 \tag{12}$$

where d_n is the inner diameter of the needle, h_{l2} is the length of the liquid in the needle, v_{l2} is the average velocity of the liquid in the cross section of the needle, p_{tn} is the pressure at the entrance of the needle, ρ_l is the density of the liquid and a_b is the acceleration of the syringe. The left-hand side of Equation 12 represents the rate of change in momentum in the needle. The right-hand side includes the rate of change in momentum as a result of the pressure difference, the effect of the syringe barrel acceleration, the viscous forces, and the rate of change in momentum as a result of the liquid entering the needle. If the needle is fully filled with $h_{l2} = L_n$, the momentum balance is expressed as shown in Equation 13.

$$\frac{d}{dt}\left(\frac{\pi}{4}d_n^2\rho_l l_n v_{l2}\right) = \frac{\pi}{4}d_n^2(p_{tn} - p_{atm}) - \frac{\pi}{4}d_n^2\rho_l a_b l_n - 8\pi\mu v_{l2} l_n \tag{13}$$

The governing equations can be reduced to a first-order system of differential equations which can be solved using a forward Euler method with the appropriate initial conditions.

This model of Zhong et al. (2021) used to evaluate the friction forces (Equation 14) offers a comprehensive framework for understanding the dy-

namics of spring-driven autoinjectors, taking into account the interactions between the barrel and the plunger. The assumptions, such as laminar flow within the needle and the effective mass of the spring, help simplify the complex physical processes involved.

$$F_f = \left[\theta_1 + \theta_2|v_p - v_b| + \theta_3\left(\frac{\pi}{4}d_b^2 p_{a-g} + F_{spring}\right)\right]\text{sign}(v_p - v_b) \tag{14}$$

In Equation 14, there are three parameters, θ_1, θ_2, and θ_3, which represent static friction, the rate of change in friction with respect to relative velocity, and the rate of change in friction with respect to the normal force acting on the plunger, respectively. When comparing the Zhong model to the Rathore model discussed in Section 3.1, the former provides a more detailed view of the internal mechanics of autoinjectors. It considers the dual movement of the plunger and barrel, which is crucial for accurate injection-time predictions. However, this complexity may also introduce additional challenges in parameter estimation and model validation.

4. Advanced Models

These models are reported in a different section as they are either more recent alternatives to the traditional models presented above or are models generally used to describe forces but have never been used in a case study on autoinjectors.

4.1. Alternative Hydrodynamic model

In this section, an alternative model for describing the the hydrodynamic forces in autoinjector devices is presented. Given that hydrodynamic forces in such systems have been extensively studied and understood, the models used to describe the them are often similar. The following model is a modified version of classical hydrodynamic expressions and differs from the standard models proposed by Verwulgen et al. (2018). The model proposed by the authors is presented in Equation 15.

$$F_{hydrodynamic} = \frac{8\pi d_b^2 \mu L}{d_n^4} + (2 + k_e)\frac{1}{2}\rho\frac{\pi d_b^6}{4d_n^4}v_b^2 \tag{15}$$

Here k_e is the dimensionless entrance loss coefficient. In Equation 15, the expression of the force necessary to overcome the pressure drop is provided.

Unlike the other models presented in the previous sections, the authors of this model included a term related to the heat losses:

$$\Delta Q = pgQ + \iint \frac{1}{2}\rho v^2 v dA + \text{heat losses} \tag{16}$$

The heat losses considered in the model are of two different types:

- heat losses localized at the entrance of the needle.
- heat losses distributed throughout the device.

The entrance losses can be defined using Equation 17 while the distributed heat losses can be described using Equation 18.

$$\Delta p_e = k_e \frac{1}{2}\rho v_n^2 \tag{17}$$

$$\Delta p_d = f\left(\frac{L_n}{d_n}\right)\frac{1}{2}\rho v_n^2 \tag{18}$$

In these equations, f is the Darcy friction factor, d_h is the diameter of the needle, L_n is the length of the needle and v is the injection velocity.

4.2. Alternative Friction models

Unlike hydrodynamic forces, which have been extensively studied over time, the description of friction forces remains more challenging. This complexity arises from the fact that friction forces are generated by microscopic phenomena, such as surface irregularities and lubricant interactions, which are difficult to observe directly. To address these challenges, various models have been developed to describe friction forces, each considering different contributing phenomena. Classic tribological theory provides a foundational framework for understanding these forces, notably through the Stribeck curve, which characterizes the relationship between friction coefficient and lubrication regimes (boundary, mixed, and hydrodynamic) as a function of lubricant viscosity, velocity, and load (Jacobson, 2003; Fernandes et al., 2016; Abdelbary and Chang, 2023). In the context of autoinjectors (AJs), these regimes are critical, as the thin lubricant layer between the syringe and stopper often operates in unknown conditions, leading to complex friction behaviour. Additionally, electro-hydrodynamic lubrication, which accounts for the influence of electric fields on lubricant flow and friction,

may be relevant for certain AJ designs with charged surfaces or specialized coatings (Chambon and Journet, 2006). These tribological concepts highlight the multifaceted nature of friction in AJ systems, where factors like lubricant displacement and surface interactions complicate predictive modelling. This section provides an overview of these models, including their integration with tribological principles, highlighting their differences and the reasons for their development.

4.2.1. LuGre model

The LuGre model, introduced by Canudas-de-Wit et al. (1995), is a general framework used to describe friction phenomena in a wide range of applications (Wang et al., 2019; Li et al., 2023; Soleimanian and Ahmadian, 2022). This model is based on the assumption that the friction force arises from the irregular microscopic interactions between two surfaces in contact. These surfaces can be conceptualised as having bristles that deform and interact in complex ways, affecting the overall frictional behaviour (Haessig and Friedland, 1991). A schematic representation of these bristles is depicted in Figure 9.

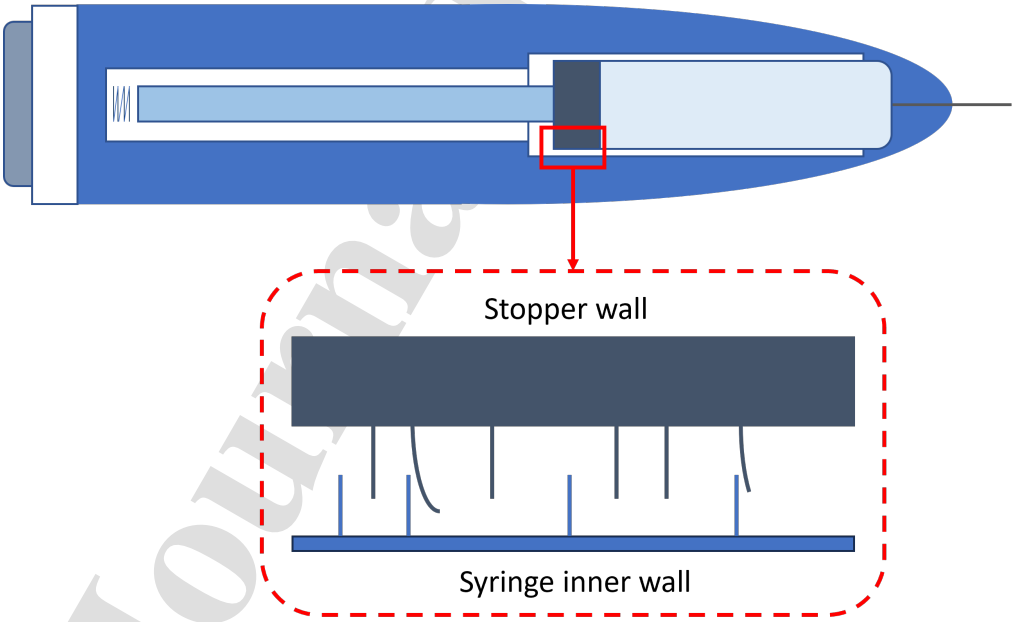

Figure 9: Bristles in two surfaces in contact with each other.

The authors developed the model starting from an expression capable to describe the average deflection of the bristles (z):

$$\frac{dz}{dt} = v_R - \frac{|v|}{g(v)}z \tag{19}$$

In this equation, v_R is the relative velocity of the bristles, and g is a positive function that depends on factors such as the material of the surfaces. Using the the average deflection of the bristles, the friction force can be defined as:

$$F_f = \sigma_0 z + \sigma_1 \frac{dz}{dt} \tag{20}$$

Here σ_0 represents the stiffness, and σ_1 is a dumping coefficient. Equation 20 can be further modified to include the effect of relative velocity:

$$F_f = \sigma_0 z + \sigma_1 \frac{dz}{dt} + \sigma_2 v_R \tag{21}$$

Equation 21 involves three parameters (σ_0, σ_1 and σ_2) and the function g. For typical friction behaviour, the function g can be expressed as:

$$\sigma_0 g(v) = F_C + (F_S + F_C)e^{(v/v_s)^2} \tag{22}$$

in this expression, F_C is the Coulomb force, F_S is the static friction force and v_s is the Stribeck velocity, i.e. the velocity at which the contact between the surfaces asperities become negligible (Daniel, 1992). For steady state systems, the relation between the friction force and the velocity is given by:

$$F_f = F_C \text{sign}(v) + (F_S - F_C)e^{-(v/v_s)^2}\text{sign}(v) + \sigma_2 v \tag{23}$$

In Equation 23, four parameters (F_C, F_S, v_s and σ_2) must be calibrated using experimental data. This calibration is crucial for accurately capturing the frictional characteristics of the surface in contact, making the LuGre model a versatile tool for describing complex friction phenomena.

4.2.2. Simplified Zhong Model

In their work, Zhong et al. (2022b) proposed an alternative model to describe the friction force in the context of injection processes. Their model was developed to separate the friction contribution fro the hydrodynamic

forces by quantifying the friction force with respect to the physical forces involved. the proposed friction model is expressed as:

$$F_f = a_0 + a_1 v + a_2 F_n \tag{24}$$

where a_0, a_1, and a_2 are constants that represent respectively the static friction, the rate of change ion the friction due to the plunger velocity and due to the normal force acting on the plunger. Moreover, the authors assumed also that the liquid velocity within the barrel is negligible such that the pressure at the bottom of the barrel is equal to the pressure in the air-gap. The normal force (F_n) acting on the syringe wall is assumed to be a fraction of the driving force F_d:

$$F_n = a_3 F_d \tag{25}$$

where a_3 is a constant representing the fraction of the driving force that is converted into the normal force. By substituting Equation 25 into Equation 24, Equation 26 is obtained.

$$F_f = a_0 + a_1 v + a_4 F_d \tag{26}$$

where the parameter a_4 is defined as the product of a_2 and a_3. This model allows for a straightforward calculation of the friction force based on the static friction, the velocity of the plunger, and the driving force.

5. Model Comparison

In the preceding sections, different models were presented to describe the forces involved in injection operations, including the approaches of Rathore (Rathore et al., 2011), Zhong (Zhong et al., 2021), and alternative methodologies such as the LuGre model (Canudas-de-Wit et al., 1995) and the Simplified Zhong model (Zhong et al., 2022b). Each of these models offers distinct perspectives on the injection process, with specific assumptions, advantages, and limitations. Before comparing their predictive performance, it is essential to clarify how the experimental data used for model calibration and validation were obtained. The following section provides a description of the experimental setup, measurement methodology, and scope of the data employed in this study.

5.1. Experimental Data and Measurement Procedure

The experimental data employed in this study were collected from controlled injection tests performed using an Instron universal testing machine (Instron, 2025) equipped with a custom fixture designed to hold the syringe in a fixed position. The experiments were conducted under constant plunger velocities to ensure reproducibility across tests. During each experiment, the plunger displacement and the corresponding extrusion force were continuously recorded. All measurements were converted into SI units prior to analysis. The dataset used for this work is composed of eight experiments, each performed at a different nominal plunger speed ranging from 120 mm/min to 600 mm/min. These tests were specifically designed for this study and are not extracted from previous publications or numerical simulations. The use of constant-velocity experiments allows isolating the frictional contribution of the stopper–barrel interface, providing a reliable basis for model calibration and comparison.

5.2. Parameter Estimation

The comparison of candidate models necessitates parameter calibration using experimental data. The set of available data is defined as

$$\mathbf{Y} = [y_1, y_2, ..., y_N] \tag{27}$$

where $\mathbf{Y}$ is the vector containing the measurements of the extrusion force, i.e. the force required to push the plunger during the injection procedure. The experimental procedure involves a systematic investigation of injection forces. For each experiment, a specific system configuration has been defined and it comprises a barrel and a stopper, along with a predetermined injection velocity. The driving force is measured using a dynamometer while the plunger advances at the selected constant velocity, enabling the acquisition of force-displacement data throughout the injection process. Table 3 shows the experimental inputs, the measured outputs, and the modelled output of the executed experiments.

The data collection involved multiple experimental runs at four different constant injection velocities;

- 120 mm/min (low injection speed)
- 192 mm/min (medium-low injection speed)

Table 3: experimental inputs , measured output and modelled output of the available dataset.

Experimental Inputs	Measured Output	Modelled Output
Velocity Barrel geometry Stopper geometry	Driving Force $[F_d]$	Hydrodynamic Force $[F_h]$ Friction Force $[F_f]$

- 300 mm/min (medium injection speed)
- 600 mm/min (high injection speed)

These velocity ranges were selected to capture the behaviour of the system across a spectrum of injection speed. Various barrel and stopper system configurations were tested to account for differences in the components provided by different providers. This approach enabled the evaluation of model performance across different physical implementations, enhancing the generalizability of the candidate calibrated models.

The difference between the measured and modelled outputs lies in their derivation. The measured output, i.e. the extrusion force, is obtained directly from the experiments, whereas the modelled output are computed using the candidate models for friction and hydrodynamic forces. This computation leverages the fact that the experimental velocity remains constant, ensuring that the sum of forces is equal to zero. The measured forces incorporate noise characterised by a covariance matrix (Σ_y). Σ_y is depended on the number of repeated measurements, n, and on the mean of the repeated measured output, $\bar{y}$, and it is evaluated using the following expression:

$$\Sigma_y = \frac{1}{1-n}\sum_{i=1}^{n}(y_i - \bar{y})(y_i - \bar{y})^T \tag{28}$$

under the assumption that the noise mean is equal to zero. To identify the optimal values of model parameters, the Maximum Likelihood (ML) estimation has been implemented. This approach identifies the optimal set of parameters ($\hat{\boldsymbol{\theta}}$) that minimizes the discrepancy between predicted and observed data distribution. The ML estimation maximizes the likelihood function, or equivalently its natural logarithm, given by:

$$\mathcal{L}(\mathbf{Y}|\hat{\theta}) = -\frac{N}{2}\left[N_y \ln(2\pi) + \ln(\det(\boldsymbol{\Sigma_y}))\right] - \frac{1}{2}\sum_{i=1}^{N}[y_i - \hat{y}_i(\theta)]^T \boldsymbol{\Sigma}_y^{-1}[y_i - \hat{y}_i(\theta)] \tag{29}$$

where N represents the sample size in dataset $\mathbf{Y}$, $\boldsymbol{\Sigma_y}$ denotes the measurement error covariance matrix, y represent the force variables during the injection procedure, $\hat{y}$ is the output vector of model predictions and $\boldsymbol{\theta}$ represents the parameter vector. The parameter estimation is achieved by solving:

$$\hat{\theta} = \arg\max_{\theta \in \Theta} \mathcal{L}(\mathbf{Y}|\hat{\theta}) \tag{30}$$

The calibration of the friction force models necessitates an indirect measurement methodology, as direct measurement of the friction force during the injection process is not feasible. The experimental friction force is obtained through the decomposition of the measured driving force according to:

$$F_f = F_d - F_h \tag{31}$$

where F_f denotes the friction force to be used in the model calibration procedure, F_d represents the experimentally acquired driving force and F_h corresponds to the computed hydrodynamic force component. This force decomposition relies on the fundamental assumption that the hydrodynamic model used to compute the hydrodynamic force accurately represents the actual hydrodynamic phenomena. A schematic representation of the calibration procedure is reported in Figure 10.

In Table 4, we present the optimal parameter values obtained through maximum likelihood estimation for each candidate friction model. The Rathore model is omitted from Table 4 as it contains no free parameters. To evaluate the statistical quality of the parameter estimates, we employ the t-test (Walpole et al., 2016). This test, with an appropriate significance level α, requires calculating the t-values for all identified parameters and comparing them with a reference t-value (Equation 32):

$$\frac{\hat{\theta}_i}{t\left(\frac{1+\alpha}{2}\right)\sqrt{\nu_{\theta,ii}}} \geq t(\alpha) \quad \forall i = 1, ..., N_\theta \tag{32}$$

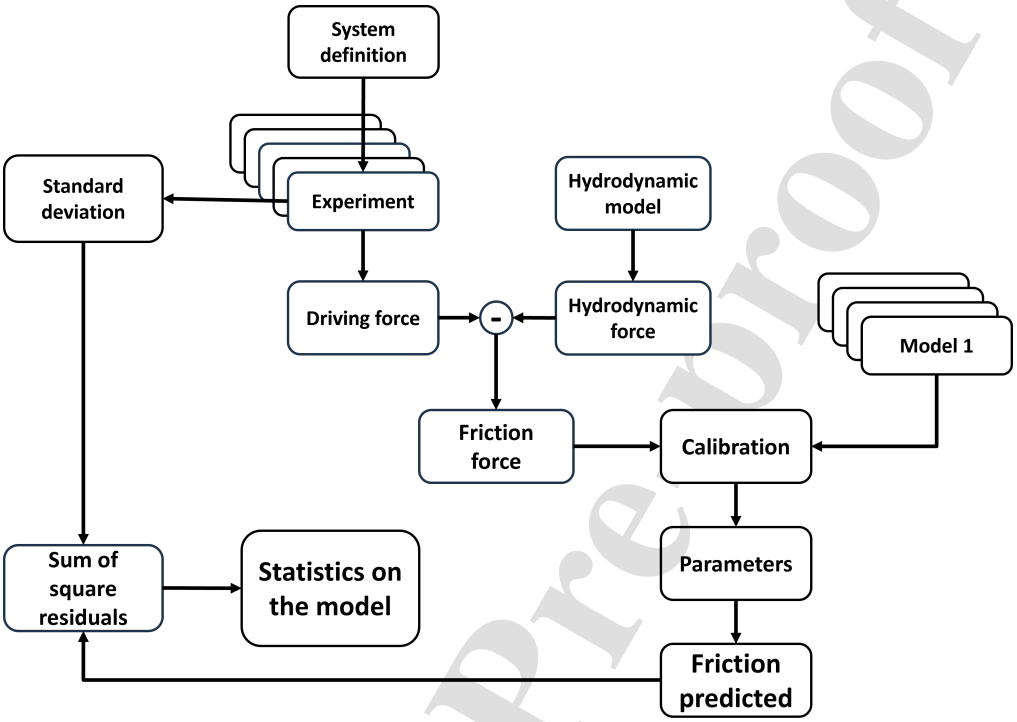

Figure 10: Calibration procedure for friction force models.

where $t(\cdot)$ represents t-values derived from a Student's distribution with degrees of freedom equal to $N \cdot N_y - N_\theta$. Here, N denotes the number of measurements, N_y the number of states, and N_θ the number of free parameters. The denominator includes the ii-element of the covariance matrix, $\nu_{\theta,ii}$, and the significance is indicated by the arguments in brackets. In Table 4 the results of this test with $\alpha = 95\%$ are shown.

For the Zhong model, all parameters (θ_1, θ_2, and θ_3) in Table 4 exhibit t-values (4.30, 184, and 4.42, respectively) that are greater than the reference t-value of 1.64. This indicates strong statistical significance for all parameters of this model, with θ_2 demonstrating exceptionally high precision in its estimation. The same happens for the parameters of the LuGre model. In contrast, the Simplified Zhong model displays mixed results. While parameter a_2 demonstrates high statistical significance with a t-value of 18.5, parameters a_1 and a_4 fail the t-test with values of 0.10 and 0.88, respectively—both below the reference threshold of 1.64. The results of the test

Table 4: Optimal parameter values for the candidate friction models obtained through maximum likelihood estimation.

Model	Parameter	Units	Optimal Value	t-ref	t-values
Zhong	θ_1	N	3.088	1.64	4.30
	θ_2	Ns/m	1.293		184
	θ_3	[-]	2.044		4.42
LuGre	F_C	N	0.999	1.64	2.46
	F_S	N	4.111		18.3
	σ_2	Ns/m	1.072		1.98
Simp. Zhong	a_1	N	-2.233	1.64	0.10
	a_2	Ns/m	0.892		18.5
	a_4	[-]	0.693		0.88

suggest that these two parameters may not be statistically significant at the chosen confidence level, indicating they could be superfluous to the model formulation. These statistical outcomes provide a quantitative basis for model selection, suggesting that the Zhong and LuGre models, with their fully significant parameter sets, may offer more reliable representations of the friction behaviour than the Simplified Zhong model in its current form.

5.3. Ranking of candidate models

When multiple models are proposed to describe a phenomenon, it is important to compare their performance in representing experimental data. Various information criteria have been proposed to help select the best model among all candidates with the assumption that the goal is to obtain an optimal balance between the fitting quality of the model and the model complexity that is represented by the number of free parameters. The Akaike Information Criteria (AIC), proposed by Akaike (1974) is a measure of this trade-off and returns a classification of the models based on their fitting performance and their complexity. The AIC index is obtained using the following equation:

$$\mathrm{AIC} = 2N_\theta - 2\mathcal{L}(\mathbf{Y}|\hat{\theta}) \tag{33}$$

where N_θ is the number of parameters, $\hat{\theta}$ are the predicted parameters obtained from the calibration procedure and $\mathcal{L}(Y|\hat{\theta})$ is the log-likelihood function defined in Equation 29. In addition to the AIC criterion, the comparison

between the distribution of the model residuals and the hypothetical distribution of the measurement error is performed. This is done implementing the χ^2-test (Silvey, 1975). This test aims to quantify the probability of observing a certain distribution of residuals under the hypothesis that the model is correctly specified (Devore, 2010). This test is based on the assumption that the model residuals obtained with $\theta = \hat{\theta}$ follow the same distribution of the measurement noise, a multivariate Gaussian distribution with zero mean and covariance Σ_y: failed for overfitting, if $\chi^2_y < \chi^2\left(\frac{1-\alpha}{2}\right)$

$$y_i - \hat{y}_i \sim \mathcal{N}(0, \Sigma_y) \tag{34}$$

Under the assumption in Equation 34 it is derived that the sum of the squared normalised residual, χ^2_y, is a random variable that is distributed as a χ^2 statistic with the appropriate degrees of freedom given by $N \cdot N_y - N_\theta$. The two-tailed test, with a given significance α has three possible outcomes: failed for overfitting, if $\chi^2_y < \chi^2\left(\frac{1-\alpha}{2}\right)$, failed for under-fitting if $\chi^2_y > \chi^2\left(\frac{1+\alpha}{2}\right)$, and passed if χ^2 lies between $\chi^2\left(\frac{1\pm\alpha}{2}\right)$ where χ^2 is evaluated using Equation 35.

$$\chi^2_y = \sum_{i=1}^{N} \left[y_i - \hat{y}_i(\hat{\theta})\right]^T \Sigma_y^{-1} \left[y_i - \hat{y}_i(\hat{\theta})\right] \sim \chi^2_{N \cdot N_y - N_{theta}} \tag{35}$$

When the test is failed for under fitting it means that the structure of the model is inappropriate to model the system under analysis. On the contrary, when the test is failed for over-fitting it means that the model includes an excessive number of free parameters. If the test is passed, the structure of the model can be considered an appropriate description of the system under analysis.

The AIC values and the χ^2-test were evaluated for all candidate models, with results presented in Table 5.

Table 5: Ranking of the models evaluated with the AIC and χ^2-test results.

Model	AIC	χ^2-test results ($\alpha = 90\%$)
Rathore	19	failed for under fitting
Zhong	50	failed for under fitting
LuGre	19	failed for under fitting
Simplified Zhong	11	passed

The Simplified Zhong model demonstrated the best performance according to the AIC criterion and the χ2-test, while the original Zhong model

showed the highest AIC value, primarily due to its large number of free parameters and inadequate fit to the system under analysis.

5.4. Comparison summary

A fundamental trade-off emerges between accuracy and simplicity across these models. The Rathore and simplified Zhong models prioritize simplicity and ease of implementation, potentially sacrificing accuracy in complex scenarios. In contrast, the detailed force balance models, such as the Zhong model, offer more precise system description at the cost of increase complexity, and the more precise description of the physical phenomena involved in the injection procedure does not always reflect in a better fitting performance. The LuGre model distinguishes itself through broad applicability, making it a versatile tool for various friction-related analysis.
Model selection should consider the specific requirements of the autoinjectors and the analytical objectives. A notable limitation common to all the discussed models is that they do not include within them the dependence o the plunger travel distance in analyse the friction force. This factor is critical for refining model accuracy and warrants for future investigation.

In the following figures (Figure 11-12) a comparison of the profiles of the friction force prediction obtained using the 4 candidate models is reported. These profiles were obtained through the process of calibration with experimental data explained earlier. To calibrate the models, 4 different experiments were performed conducted at velocities of 0.0020, 0.0032, 0.0050 and 0.01 m/s, which remains constant throughout the duration of the experiment.

In addition to the plots in Figures 11-12 the parity plots used to compare the predicted friction force with the measured friction are reported in Figures 13-14. These figures show that the Rathore model consistently overestimates the friction force, whereas the Simplified Zhong model provides the best agreement with the experimental data, as it accounts for the spatial variation of the friction force. In contrast, the other models only consider velocity dependence and neglect the variation of friction with the travelled distance.

Table 6 provides a comprehensive comparison of model characteristics, facilitating systematic evaluation based on implementation complexity, features, practical aspects, accuracy, reliability, and limitations. This comparative framework enables informed selection of appropriate models for specific applications while highlighting areas requiring further development.

Table 6: Model Comparison.

Feature	Rathore	Zhong	Alt. Hydro	LuGre	Simp. Zhong
Implementation Complexity					
Easy to implement	✓	×	×	×	✓
Simple parameter estimation	✓	×	×	×	✓
Requires numerical solutions	×	✓	✓	✓	×
Model Features					
Accounts for dual movement	×	✓	×	×	✓
Heat loss consideration	×	×	✓	×	×
Microscopic friction analysis	×	×	×	✓	×
Linear force relationships	✓	×	×	×	✓
Practical Aspects					
Extensive validation required	×	✓	✓	✓	×
Broad applicability	×	✓	✓	✓	×
Real-time calculations	✓	×	×	×	✓
Accuracy & Reliability					
High accuracy in complex cases	×	✓	✓	✓	×
Robust to parameter variations	✓	×	×	×	✓
Validated across materials	×	✓	✓	✓	×
Limitations					
Assumes constant friction	✓	×	×	×	✓
Requires extensive data	×	✓	✓	✓	×
Limited by assumptions	✓	×	×	×	✓

Legend: ✓: Yes/Present, ×: No/Absent

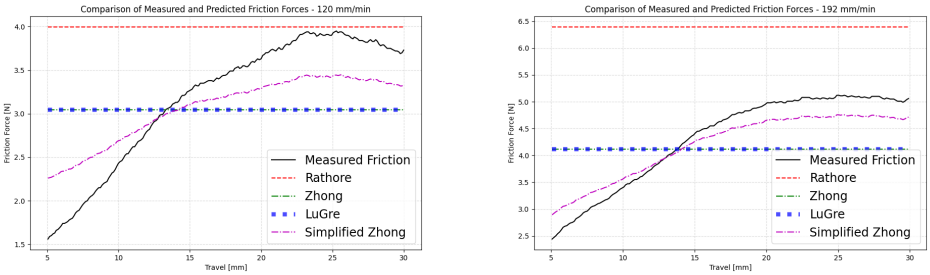

(a) (b)

Figure 11: Comparison of the friction force profiles obtained using the described models with the experimental data collected from experiments at constant velocities equal to (a) 0.0020 m/s and (b) 0.0032 m/s.

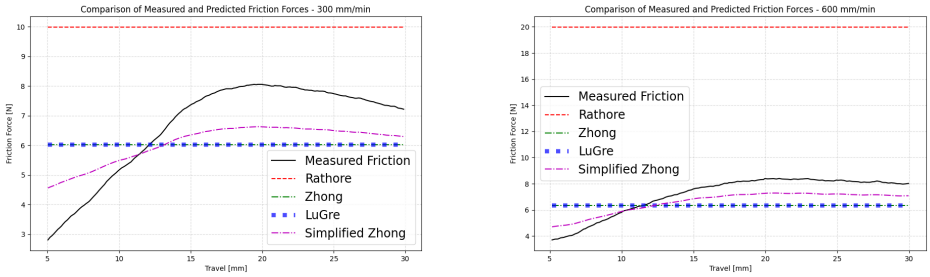

(a) (b)

Figure 12: Comparison of the friction force profiles obtained using the described models with the experimental data collected from experiments at constant velocities equal to (a) 0.0050 m/s and (b) 0.0100 m/s.

6. Evaluation of the Injection Time

The injection time is the critical parameter in autoinjector performance evaluation and can be derived using momentum balance principles. In this approach, the driving force is provided by the compressed spring (Equation 37), while the resistive forces are calculated using the models described in previous sections (Section 3-4). The momentum balance equation to determine the injection time can be expressed as

$$m\frac{d^2x}{dt^2} = F_d - F_f - F_h \tag{36}$$

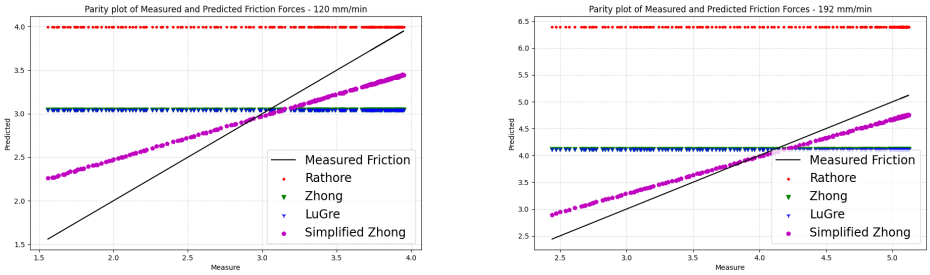

(a) (b)

Figure 13: Parity plots of measured vs. predicted friction forces at constant velocities of (a) 0.0020 m/s and (b) 0.0032 m/s for the different models.

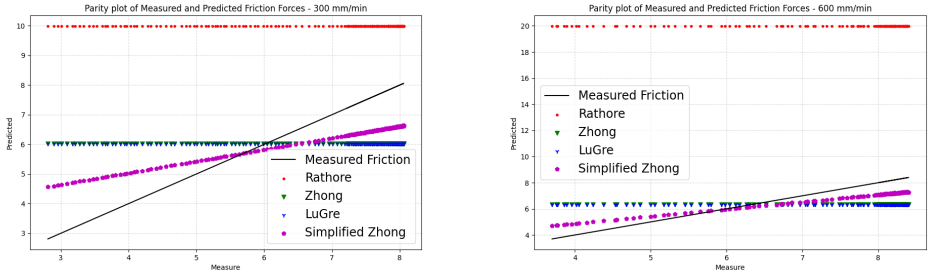

(a) (b)

Figure 14: Parity plots of measured vs. predicted friction forces at constant velocities of (a) 0.0050 m/s and (b) 0.0100 m/s for the different models.

$$F_d = k(l_0 - x) \tag{37}$$

The following table presents the physical parameters used in the in silico implementation of the models presented in Section 3-4. These parameters characterise the spring-driven mechanism, the plunger geometry, and the fluid properties that govern the injection dynamics. The model incorporates the spring force, viscous damping of the oil film between the plunger and barrel, and the hydrodynamic resistance of the drug formulation flowing through the needle. These parameters were used to simulate the temporal profile of the plunger travel and calculate the total injection time.

Figures 15 and 16 compare the injection time profiles obtained using the four different models for the friction forces (Rathore, Simplified Zhong, Lu-

Table 7: Parameters used for in-silico model

Parameter	Value	Unit
Spring constant (k)	100	N/m
Spring compression (l_0)	50	mm
Initial plunger position (x_0)	0	mm
Final plunger position (x_{final})	40	mm
Oil viscosity (μ_{oil})	0.05	-
Plunger radius (r_b)	5	mm
Plunger length ($l_{stopper}$)	5	mm
Oil film thickness (d_{oil})	0.1	mm
Fluid viscosity (μ_F)	0.003	-
Needle length (L_n)	15	mm
Needle radius (r_n)	0.25	mm
Plunger mass ($m_{stopper}$)	5	g

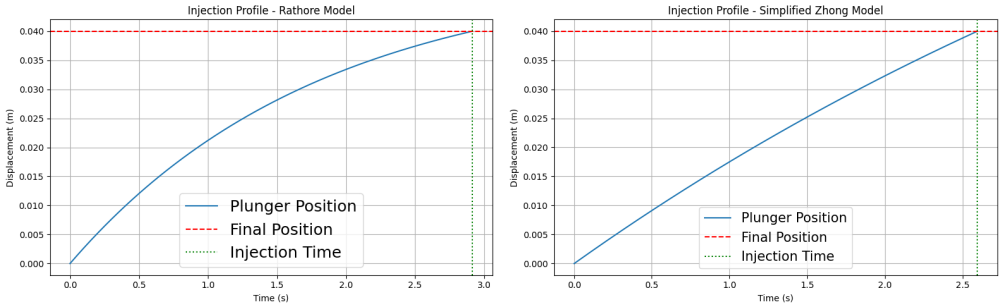

(a) (b)

Figure 15: Comparison of Injection Profiles for (a) Rathore Model and (b) Simplified Zhong Model. The graphs show the plunger position (blue line) over time, with the final position (red dashed line) and injection time (green dotted line) indicated for each model.

Gre, and Zhong, see Section 3-4 for further details) simulated in a Python framework. The profiles display the plunger displacement over time (y-axis) with target position(red line). Using the Rathore model for the friction force (Figure 15a), the plunger reaches the final displacement (x=0.04 m) in 2.7 seconds with an exponential profile. As outlined in Section 3.1, in the momentum balance (Equation 6, this model uses linear friction an hydrodynamic forces balancing the driving forces to enable the injection. Using the Simplified Zhong Model (Section 4.2.2) the plunger achieves the target

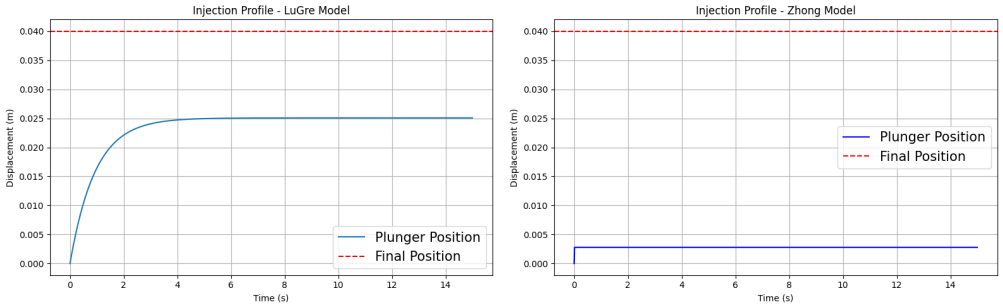

(a) (b)

Figure 16: Comparison of Injection Profiles for (a) LuGre Model and (b) Zhong Model. The graphs show the plunger position (blue line) over time, with the final position (red dashed line) and injection time indicated for each model.

position in 2.5 s showing a near-linear displacement profile (Figure 15b). For the injection time evaluated using the LuGre friction model (Figure 16) the plunger reaches only 0.025m of displacement in 15 seconds, failing to inject fully. This is due to the fact that using the parameters reported in Table 4 the friction force is overestimated and this causes excessive resistance, stalling the plunger. The same phenomenon occurs with the Zhong model, Section 3.2. Figure 16 shows negligible movement of the plunger, remaining at 0.001m for 15 seconds without reaching the target displacement. These simulation results show the critical influence of model selection on injection-time predictions. The Rathore and Simplified Zhong models yield complete injections within practical time frames (2.7 and 2.5 seconds, respectively), demonstrating their utility in autoinjector design applications. In contrast, when implemented with the parameters of Table 7, the LuGre and Zhong models generate excessive friction force estimates that prevent complete plunger travel even over extended periods. This comparative analysis highlights the importance of selecting an appropriate model and accurately calibrating its parameters when assessing autoinjector performance, as overestimating the friction force can significantly skew predictions of device behaviour and potentially prompt unnecessary design changes. Examination of force profiles from the LuGre and Zhong models reveals performance discrepancies. For the LuGre model (Figure 17a), the spring force peaks at 7 N and falls to 0 N in 1 s, the friction force decreases from 7 N to 0.5 N, and the Hydrodynamic Force holds at 6 N, correlating with limited displacement

of 0.025m over 15 s due to initial high friction. For the Zhong model (Figure 17b), the spring force peaks at 5 N and drops to 0 N after 2 s, while the Friction Force remains constant at 2.5 N and the hydrodynamic force stays at 6 N, contributing to plunger stalling at 0.001m due to excessive resistance. These profiles highlight the need for model refinement and precise parameter calibration to address overestimated frictional and hydrodynamic forces, ensuring accurate injection time predictions.

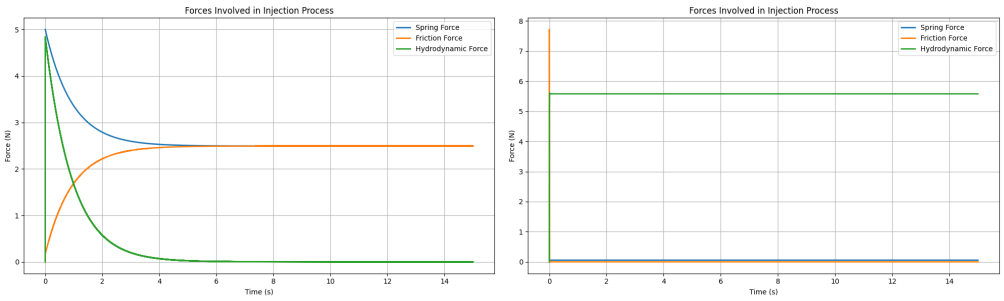

(a) (b)

Figure 17: Force profiles over time for (a) LuGre and (b) Zhong model during the injection process. The blue line represents the spring force, the orange line the friction force and the green line the hydrodynamic force.

However, a key limitation of the models lies in the dataset used for parameter calibration. In the experimental dataset, friction forces were observed to increase along the plunger travel, a position-dependent behaviour not accounted for in the current models. Consequently, these models are likely to perform better for systems where friction is independent of the distance travelled by the stopper, as the assumption of constant friction simplifies parameter estimation and improves predictive accuracy.

7. Future Perspectives

7.1. Future Research Areas

The main area for future development lies in improving the accuracy of existing mathematical models used to predict friction forces in autoinjector devices. Current models often rely on simplifying assumptions that may not hold under varying materials, lubrication states, or device geometries. Future research should aim to develop more generalised frameworks that can

capture the non-linear and dynamic nature of friction under realistic operating conditions. One promising direction is the inclusion of additional physical variables currently neglected in most models, such as the plunger travel distance and the local contact deformation between the stopper and barrel. Incorporating these parameters would allow the prediction of the evolution of friction throughout the injection process rather than assuming a constant or quasi-static behaviour. Moreover, Machine Learning (ML) and hybrid modelling approaches can significantly enhance predictive capability. For example, ML algorithms such as Gaussian Processes (GPs), Random Forests, or Artificial Neural Networks (ANNs) have been used in other fields to model unknown phenomena in different fields (add references) and could be trained on experimental datasets to capture the non-linear relationships between friction and input features (i.e., material properties, temperature, injection speed, and lubricant degradation). Hybrid models could combine a first-principles core describing macroscopic dynamics (i.e., force balance and motion equations) with a data-driven component correcting the microscopic effects that are not modelled in the first-principles model, such as viscoelastic deformation or local adhesion phenomena (Friso et al., 2024). Another crucial area for future investigation involves accounting for patient variability. Friction behaviour can indirectly influence injection time, which depends also on patient-dependent parameters such as tissue back pressure and environmental conditions. Integrating stochastic or population-based approaches, such as Monte Carlo simulations or Bayesian hierarchical models, could allow the quantification of uncertainty and the prediction of device performance across diverse patient populations. From a practical point of view, these modelling efforts require comprehensive datasets for model training and validation. Such datasets should include systematic measurements of friction forces under varying conditions (temperature, humidity, material batches, lubricant types, ageing effects, and repeated use). Additionally, coupling friction measurements with high-speed imaging and surface characterisation (i.e., roughness and lubrication integrity) would enable the development of multi-scale models linking microscopic interactions to macroscopic performance. Finally, the development of multi-physics and multi-scale models remains an ambitious yet highly valuable goal. These models could simultaneously account for mechanical, thermal, and fluidic interactions within the autoinjector system, providing a full representation of its performance. Such integrated frameworks, supported by experimental data and data-driven corrections, will lead to more robust, reliable, and patient-tailored autoinjector

designs.

8. Conclusion

8.1. Summary of Main Results

This review article has explored and evaluated various models in the literature that describe the forces involved in injection procedures. Each model exhibits unique strengths and weaknesses. To summarise:

- **Rathore model:** valued for its simplicity and linear relationship, but limited by assumptions regarding lubrication uniformity and material specificity.
- **Zhong model:** offers a comprehensive and detailed representation of the autoinjector mechanism, including the dual movement of barrel and plunger, yet is complex and sensitive to parameter estimation.
- **Alternative hydrodynamic model:** increases accuracy over standard models by incorporating distributed and entrance loss coefficients, at the cost of increased complexity.
- **LuGre model:** provides a versatile approach for modelling friction forces, though it necessitates extensive calibrations.
- **Simplified Zhong model:** simplifies friction phenomena modelling, facilitating easier implementation but potentially overlooking critical accuracy factors such as pre-sliding hysteresis, stick–slip transitions, and velocity-dependent behaviours at low speeds.

8.2. Practical Implications

For researchers and designers of autoinjectors, this review aimed to evaluate the performance of different studied models and understand their applicability in different contexts. The findings highlight that there is no universal model capable of describing frictional behaviour under all systems (barrel and stopper combinations) and injection velocities. Instead, the choice of model should depend on the specific stage and objective of the design process. Simpler models such as the Rathore and Simplified Zhong models are advantageous during early design phases or when fast estimations are required, as they provide good interpretability and limited computational cost. Conversely, more complex models, such as the Zhong, LuGre, or hydrodynamic

formulations, are better suited for high-fidelity simulations and the optimisation of final device performance, where friction dynamics and material-specific effects must be captured accurately. This review also highlights the importance of validating these models across various materials and operating conditions to ensure their robustness. Enhancing parameter estimation strategies and developing standardised validation protocols are crucial next steps. Finally, integrating first-principles and data-driven approaches represents a promising route to balance interpretability with predictive accuracy in future autoinjector design.

8.3. Final Remarks

This review of autoinjector modelling reveals significant advances alongside persistent challenges. Existing models effectively capture basic mechanical interactions but struggle to reproduce dynamic friction forces accurately. Researchers should select a modelling framework based on the required balance between simplicity, interpretability, and predictive precision. Simplified models remain valuable tools for preliminary analysis and design screening, while advanced or hybrid models are essential when precision and generality are prioritised. Although no single model can fully capture the complex non-linear behaviour of friction, each provides useful insights into specific aspects of the injection process. In conclusion, while considerable progress has been made in understanding and modelling the forces acting in autoinjector mechanisms, further research is needed to bridge the gap between simplicity and accuracy. By consolidating current knowledge and identifying key limitations, this work lays the foundation for more targeted investigations. Future developments should aim to integrate real-time analytics, uncertainty quantification, and machine learning, enabling adaptive and patient-specific modelling of injection performance.

Acknowledgements

The authors gratefully acknowledge the support of the Department of Chemical Engineering at University College London and GSK.

References

Abdelbary, A., Chang, L., 2023. 7 - lubrication and surface engineering, in: Abdelbary, A., Chang, L. (Eds.), Principles of Engineering Tribology. Academic Press, pp. 295–343.

Akaike, H., 1974). A new look at the statistical model identification. IEEE Transactions on Automatic Control 19, 716–723.

Al-Bender, F., 2010. Fundamentals of friction modeling. Proceedings - ASPE Spring Topical Meeting on Control of Precision Systems, ASPE 2010 48.

Allmendinger, A., Fischer, S., Huwyler, J., Mahler, H.C., Schwarb, E., Zarraga, I.E., Mueller, R., 2014. Rheological characterization and injection forces of concentrated protein formulations: An alternative predictive model for non-newtonian solutions. European Journal of Pharmaceutics and Biopharmaceutics 87, 318–328. doi:https://doi.org/10.1016/j.ejpb.2014.01.009.

Badkar, A.V., Gandhi, R.B., Davis, S.P., LaBarre, M.J., 2021. Subcutaneous delivery of high-dose/volume biologics: Current status and prospect for future advancements. Drug Design, Development and Therapy 15, 159–170. doi:10.2147/DDDT.S287323. pMID: 33469268.

Barone, D., Singer, B., Merkov, L., Rametta, M., Suarez, G., 2016. Survey of us patients with multiple sclerosis: Comparison of the new electronic interferon beta-1b autoinjector (betaconnect™) with mechanical autoinjectors. Neurology and Therapy 5.

Canudas-de-Wit, C., Olsson, H., Astrom, K., Lischinsky, P., 1995. A new model for control of systems with friction. IEEE Transactions on Automatic Control 40, 419–425. doi:10.1109/9.376053.

Chambon, L., Journet, B., 2006. Modelling of fretting fatigue in a fracture-mechanics framework. Tribology International 39, 1220–1226. The Fourth International Symposium on Fretting Fatigue.

Daniel, R., 1992. Control of machines with friction: Brian armstrong-hélouvry. Automatica 28, 1285–1287. doi:https://doi.org/10.1016/0005-1098(92)90076-R.

Derakhshandeh, R., Meyers, B.A., Zhang, J., Veilleux, J.C., 2025. Subcutaneous depot formation and diffusion in autoinjector delivery: insights from high-speed synchrotron imaging. International Journal of Pharmaceutics 681, 122975.

Devore, J.L., 2010. Probability and Statistics for Engineering and the Sciences. Cengage Learning, Inc, Boston, MA, 8th edition.

Dostal, P., Taubel, J., Lorch, U., Aggarwal, V., York, T., 2023. The reliability of auto-injectors in clinical use: A systematic review. Cureus 15, e41601.

Dribin, T.E., Waserman, S., Turner, P.J., 2023. Who needs epinephrine? anaphylaxis, autoinjectors, and parachutes. The Journal of Allergy and Clinical Immunology: In Practice 11, 1036–1046. doi:https://doi.org/10.1016/j.jaip.2023.02.002.

Fernandes, C.M., Martins, R.C., Seabra, J.H., 2016. Coefficient of friction equation for gears based on a modified hersey parameter. Tribology International 101, 204–217.

Fischer, I., Schmidt, A., Bryant, A., Besheer, A., 2015. Calculation of injection forces for highly concentrated protein solutions. International Journal of Pharmaceutics 493, 70–74. doi:https://doi.org/10.1016/j.ijpharm.2015.07.054.

Fox, J.G., Mahanty, J., 1970. The Effective Mass of an Oscillating Spring. American Journal of Physics 38, 98–100. doi:10.1119/1.1976240.

Friso, A., Palmer, M., Bano, G., Galvanin, F., 2024. On the development of hybrid models to describe delivery time in autoinjectors, in: Manenti, F., Reklaitis, G.V. (Eds.), 34th European Symposium on Computer Aided Process Engineering / 15th International Symposium on Process Systems Engineering. Elsevier. volume 53 of *Computer Aided Chemical Engineering*, pp. 157–162. doi:https://doi.org/10.1016/B978-0-443-28824-1.50027-2.

Haessig, D. A., J., Friedland, B., 1991. On the Modeling and Simulation of Friction. Journal of Dynamic Systems, Measurement, and Control 113, 354–362. doi:10.1115/1.2896418.

Instron, 2025. 6800 series universal testing systems. URL: `https://www.instron.com/en/`. accessed: 2025-04-03.

Jacobson, B., 2003. The stribeck memorial lecture. Tribology International 36, 781–789. NORDTRIB symposium on Tribology 2002.

Kennelly, T.R., Eshraghi, J., Dabiri, S., Vlachos, P.P., 2024. An experimentally validated cavitation inception model for spring-driven autoinjectors. International Journal of Pharmaceutics 652, 123753. doi:https://doi.org/10.1016/j.ijpharm.2023.123753.

Li, D., Hu, X., Yu, S., Deng, S., Yan, M., Sun, F., Song, J., Tang, L., 2020. Silence of lncrna miat-mediated inhibition of dlg3 promoter methylation suppresses breast cancer progression via the hippo signaling pathway. Cellular Signalling 73.

Li, J., Lu, Y., He, F., Miao, L., 2023. Motion control of hydraulic actuators with nonlinear friction compensation: Applied to variable valve systems of diesel engine. ISA Transactions 137, 561–573.

Masciopinto, V., 2024. Shl medical's elexy™: Redefining possibilities. ONdrugDelivery , 78–82.

McCawley, M., Lavin, A., 2023. Gas-powered autoinjector platform enables biologics drug delivery. ONdrugDelivery 152, 57–60.

Ong, K.L., Stafford, L.K., 2023. Global, regional, and national burden of diabetes from 1990 to 2021, with projections of prevalence to 2050: a systematic analysis for the global burden of disease study 2021. The Lancet 402, 203–234. doi:https://doi.org/10.1016/S0140-6736(23)01301-6.

Pritchard, P., 2010. Fox and McDonald's Introduction to Fluid Mechanics, 8th Edition. John Wiley & Sons.

Rathore, N., Pranay, P., Eu, B., Ji, W., Walls, E., 2011. Variability in syringe components and its impact on functionality of delivery systems. PDA Journal of Pharmaceutical Science and Technology 65, 468–480. doi:10.5731/pdajpst.2011.00785.

Ravi, A., Sadhna, D., Nagpaal, D., Chawla, L., 2015. Needle free injection technology: A complete insight. International Journal of Pharmaceutical Investigation 5, 192. doi:10.4103/2230-973x.167662.

Renukuntla, J., Vadlapudi, A.D., Patel, A., Boddu, S.H., Mitra, A.K., 2013. Approaches for enhancing oral bioavailability of peptides and proteins. International Journal of Pharmaceutics 447, 75–93.

Riesz, P., Kondo, T., 1992. Free radical formation induced by ultrasound and its biological implications. Free Radical Biology and Medicine 13, 247–270.

Ross, A.P., Nicholas, J.A., Tai, M.H., Yeung, S., Shaikh, N.F., Chen, H., Fernandes, M., Cortright, A., Hawkins, K., 2025. Real-world satisfaction and experience with injection and autoinjector device for ofatumumab indicated for multiple sclerosis. BMC Neurology 25.

Rowley, W.R., Bezold, C., Arikan, Y., Byrne, E., Krohe, S., 2017. Diabetes 2030: Insights from yesterday, today, and future trends. Population Health Management 20, 6–12. doi:10.1089/pop.2015.0181. pMID: 27124621.

Roy, A., Geetha, R.V., Magesh, A., Vijayaraghavan, R., Ravichandran, V., 2021. Autoinjector – a smart device for emergency cum personal therapy. Saudi Pharmaceutical Journal 29, 1205–1215. doi:https://doi.org/10.1016/j.jsps.2021.09.004.

Scherer, T.M., Liu, J., Shire, S.J., Minton, A.P., 2010. Intermolecular interactions of igg1 monoclonal antibodies at high concentrations characterized by light scattering. The Journal of Physical Chemistry B 114, 12948–12957. doi:10.1021/jp1028646. pMID: 20849134.

Schneider, A., Jost, R., Jordi, C., Lange, J., 2023. Autoinjectors for large-volume subcutaneous drug delivery: a review of current research and future directions. Expert Opinion on Drug Delivery 20, 815–830. doi:10.1080/17425247.2023.2219891.

Shaik, S., Pasha, M., Mehar, A., 2016. Strength based design of compression springs for auto-injector syringes doi:10.4010/2016.1418.

Shilpa, S., C.M.P, S., Prashob, G.R., S., S., 2022. Auto injectors & pen injectors: A user-centric deisgn approach. Zenodo doi:https://doi.org/10.5281/zenodo.6925021.

Sicherer, S.H., Simons, F.E.R., the Section on Allergy, Immunology, 2007. Self-injectable epinephrine for first-aid management of anaphylaxis. Pediatrics 119, 638–646. doi:10.1542/peds.2006-3689.

Silvey, S., 1975. Statistical Inference. Routledge.

Simons, K.J., Simons, F.E.R., 2010. Epinephrine and its use in anaphylaxis: Current issues. Current Opinion in Allergy and Clinical Immunology 10, 354 – 361. doi:10.1097/ACI.0b013e32833bc670. cited by: 167.

Soleimanian, P., Ahmadian, H., 2022. Modeling friction effects in lubricated roller guideways using a modified lugre model. Journal of Vibration and Control 28, 2519–2530. arXiv:https://doi.org/10.1177/10775463211013922.

Sree, V., Zhong, X., Bilionis, I., Ardekani, A., Tepole, A.B., 2023. Optimizing autoinjector devices using physics-based simulations and gaussian processes. Journal of the Mechanical Behavior of Biomedical Materials 140, 105695. doi:https://doi.org/10.1016/j.jmbbm.2023.105695.

Stiefel, G., Kakleas, K., Luyt, D., 2020. Adrenaline autoinjectors: an update of the last decade. Paediatrics and Child Health 30, 249–254. doi:https://doi.org/10.1016/j.paed.2020.04.002.

Thueer, T., Birkhaeuer, L., Reilly, D., 2018. Development of an advanced injection time model for an autoinjector. Medical Devices: Evidence and Research 11, 215–224. doi:10.2147/MDER.S151727.

Torisu, T., Maruno, T., Hamaji, Y., Ohkubo, T., Uchiyama, S., 2017. Synergistic effect of cavitation and agitation on protein aggregation. Journal of Pharmaceutical Sciences 106, 521–529.

Verwulgen, S., Beyers, K., Van Mulder, T., Peeters, T., Truijen, S., Dams, F., Vankerckhoven, V., 2018. Assessment of forces in intradermal injection devices: Hydrodynamic versus human factors. Pharmaceutical Research 35. doi:10.1007/s11095-018-2397-2.

Walpole, R., Myers, S., Myers, R., Ye, K., 2016. Probability Statistics for Engineers Scientists Global Edition. Pearson Deutschland.

Wang, X., Lin, W., Ji, X., Gao, Z., Bai, X., Guo, Y., 2019. Dynamic analysis of a planar multibody system with multiple revolute clearance joints. Proceedings of the Institution of Mechanical Engineers, Part C 233, 3429–3443. arXiv:https://doi.org/10.1177/0954406218819022.

Zarraga, I.E., Taing, R., Zarzar, J., Luoma, J., Hsiung, J., Patel, A., Lim, F.J., 2013. High shear rheology and anisotropy in concentrated solutions

of monoclonal antibodies. Journal of Pharmaceutical Sciences 102, 2538–2549. doi:https://doi.org/10.1002/jps.23647.

Zhong, X., Bilionis, I., Ardekani, A.M., 2022a. A framework to optimize spring-driven autoinjectors. International Journal of Pharmaceutics 617, 121588. doi:https://doi.org/10.1016/j.ijpharm.2022.121588.

Zhong, X., Guo, T., Vlachos, P., Veilleux, J.C., Shi, G.H., Collins, D.S., Ardekani, A.M., 2021. An experimentally validated dynamic model for spring-driven autoinjectors. International Journal of Pharmaceutics 594, 120008. doi:https://doi.org/10.1016/j.ijpharm.2020.120008.

Zhong, X., Mitra, H., Veilleux, J.C., Simmons, E., Shi, G.H., Ardekani, A.M., 2022b. The role of liquid rheological properties on the injection process of a spring-driven autoinjector. International Journal of Pharmaceutics 628, 122296. doi:https://doi.org/10.1016/j.ijpharm.2022.122296.

Zhong, X., Veilleux, J.C., Shi, G.H., Collins, D.S., Vlachos, P., Ardekani, A.M., 2023. Hydrodynamic considerations for spring-driven autoinjector design. International Journal of Pharmaceutics 640, 122975. doi:https://doi.org/10.1016/j.ijpharm.2023.122975.

UCL CHEMICAL ENGINEERING
Prof Federico Galvanin
Professor of Chemical Engineering
PhD, FHEA, AMIChemE
Torrington Place
London WC1E 7JE
Tel. +44 (0)20 7679 5739
e-mail: f.galvanin@ucl.ac.uk

02 December 2025

"*Mathematical Modelling of Injection Time in Autoinjectors: State of the Art and Future Perspectives*"

Highlights

- Reviews mathematical models for injection time in autoinjectors
- Compares models' accuracy, complexity and performance
- Highlights the need for distance-dependent friction modelling
- Suggests machine learning applications for future autoinjector design

Please do not hesitate to contact me at f.galvanin@ucl.ac.uk for any additional clarification. proc

I thank you for your consideration and look forward to hearing from you.

Sincerely,

Federico Galvanin

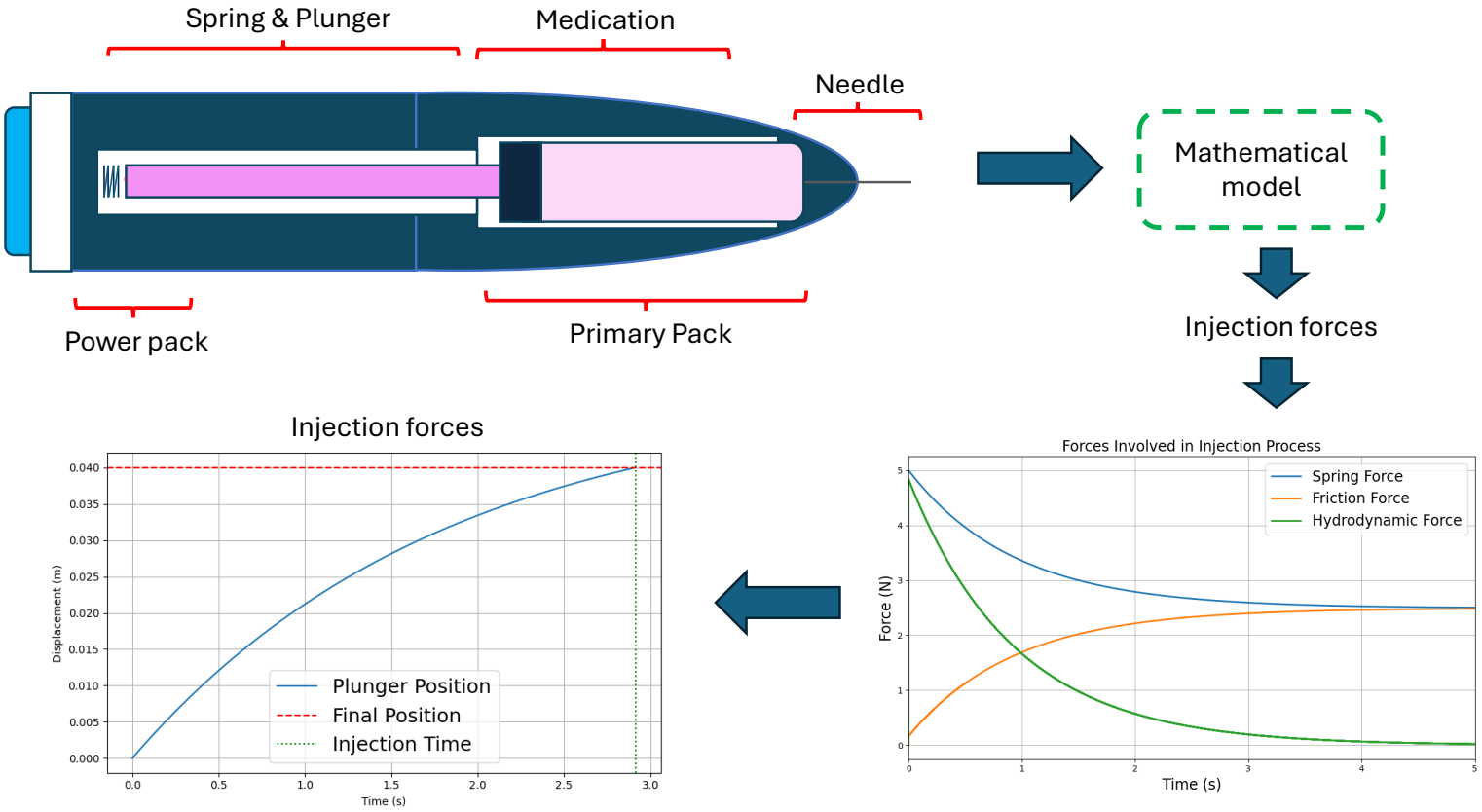

Declaration of interests

☒ The authors declare that they have no known competing financial interests or personal relationships that could have appeared to influence the work reported in this paper.

☐The authors declare the following financial interests/personal relationships which may be considered as potential competing interests: